Engineering photonic nanojets

Myun-Sik Kim,[1,*] Toralf Scharf,[1] Stefan Mühlig,[2] Carsten Rockstuhl,[2] and Hans Peter Herzig[1]

[1]*Optics & Photonics Technology Laboratory, Ecole Polytechnique Fédérale de Lausanne (EPFL), Neuchâtel, CH-2000, Switzerland*

[2]*Institute of Condensed Matter Theory and Solid State Optics, Abbe Center of Photonics, Friedrich-Schiller-Universität Jena, 07743 Jena, Germany*

[*]*myunsik.kim@epfl.ch*

Abstract: Photonic Nanojets are highly localized wave fields emerging directly behind dielectric microspheres; if suitably illuminated. In this contribution we reveal how different illumination conditions can be used to engineer the photonic Nanojets by measuring them in amplitude and phase with a high resolution interference microscope. We investigate how the wavelength, the amplitude distribution of the illumination, its polarization, or a break in symmetry of the axial-symmetric structure and the illumination affect the position, the localization and the shape of the photonic Nanojets. Various fascinating properties are systematically revealed and their implications for possible applications are discussed.

OCIS codes: (180.3170) Interference microscopy; (290.4020) Mie theory; (140.3300) Laser beam shaping; (120.2880) Holographic interferometry.

References and links

1. G. Mie, "Beiträge zur optik trüber medien, speziell kolloidaler metallösungen," Ann. Phys. **25**, 377–445 (1907).
2. H. C. Van de Hulst, *Light Scattering by Small Particles* (Dover, 1981), Chap. 9.
3. A. Heifetz, S.-C. Kong, A. V. Sahakian, A. Taflove, and V. Backman, "Photonic nanojets," J Comput Theor Nanosci **6**(9), 1979–1992 (2009).
4. Z. Chen, A. Taflove, and V. Backman, "Photonic nanojet enhancement of backscattering of light by nanoparticles: a potential novel visible-light ultramicroscopy technique," Opt. Express **12**(7), 1214–1220 (2004).
5. X. Li, Z. Chen, A. Taflove, and V. Backman, "Optical analysis of nanoparticles via enhanced backscattering facilitated by 3-D photonic nanojets," Opt. Express **13**(2), 526–533 (2005).
6. C. M. Ruiz and J. J. Simpson, "Detection of embedded ultra-subwavelength-thin dielectric features using elongated photonic nanojets," Opt. Express **18**(16), 16805–16812 (2010).
7. P. Ferrand, J. Wenger, A. Devilez, M. Pianta, B. Stout, N. Bonod, E. Popov, and H. Rigneault, "Direct imaging of photonic nanojets," Opt. Express **16**(10), 6930–6940 (2008).
8. A. Devilez, N. Bonod, J. Wenger, D. Gérard, B. Stout, H. Rigneault, and E. Popov, "Three-dimensional subwavelength confinement of light with dielectric microspheres," Opt. Express **17**(4), 2089–2094 (2009).
9. C. Rockstuhl, I. Märki, T. Scharf, M. Salt, H. P. Herzig, and R. Dändliker, "High resolution interference microscopy: a tool for probing optical waves in the far-field on a nanometric length scale," Curr. Nanosci. **2**(4), 337–350 (2006).
10. M.-S. Kim, T. Scharf, and H. P. Herzig, "Small-size microlens characterization by multiwavelength high-resolution interference microscopy," Opt. Express **18**(14), 14319–14329 (2010).
11. J. Schwider, R. Burow, K.-E. Elssner, J. Grzanna, R. Spolaczyk, and K. Merkel, "Digital wave-front measuring interferometry: some systematic error sources," Appl. Opt. **22**(21), 3421–3432 (1983).
12. P. Hariharan, B. F. Oreb, and T. Eiju, "Digital phase-shifting interferometry: a simple error-compensating phase calculation algorithm," Appl. Opt. **26**(13), 2504–2506 (1987).
13. C. Rockstuhl, M. Salt, and H. P. Herzig, "Theoretical and experimental investigation of phase singularities generated by optical micro- and nano-structures," J. Opt. A, Pure Appl. Opt. **6**(5), 271–276 (2004).
14. M. Born and E. Wolf, *Principles of Optics* (Cambridge University Press, 1999), 7th ed.
15. E. Abbe, "Beiträge zur theorie des mikroskops und der mikroskopischen wahrnehmung," Arch. Mikrosk. Anat. Entw. Mech **9**, 413–468 (1873).
16. H. Köhler, "On Abbe's theory of image formation in the microscope," Opt. Acta (Lond.) **28**, 1691–1701 (1981).
17. H. Gross, H. Zugge, M. Peschka, and F. Blechinger, *Handbook of Optical Systems* (Wiley, 2007) Vol. 3, p. 126.
18. W. Singer, M. Totzeck, and H. Gross, *Handbook of Optical Systems* (Wiley, 2005) Vol. 2, p. 410.
19. F. Gori, G. Guattari, and C. Padovani, "Bessel-Gauss beams," Opt. Commun. **64**(6), 491–495 (1987).
20. J. Durnin, J. J. Miceli, Jr., and J. H. Eberly, "Diffraction-free beams," Phys. Rev. Lett. **58**(15), 1499–1501 (1987).

#145428 - $15.00 USD Received 5 Apr 2011; revised 29 Apr 2011; accepted 2 May 2011; published 9 May 2011

21. G. Indebetouw, "Nondiffracting optical-fields - some remarks on their analysis and synthesis," J. Opt. Soc. Am. A **6**(1), 150–152 (1989).
22. M. Stalder and M. Schadt, "Linearly polarized light with axial symmetry generated by liquid-crystal polarization converters," Opt. Lett. **21**(23), 1948–1950 (1996).
23. R. Dorn, S. Quabis, and G. Leuchs, "Sharper focus for a radially polarized light beam," Phys. Rev. Lett. **91**(23), 233901 (2003).
24. M.-S. Kim, T. Scharf, S. Mühlig, C. Rockstuhl, and H. P. Herzig, "Gouy phase anomaly in photonic nanojets," Appl. Phys. Lett. (accepted for publication).
25. A. Devilez, B. Stout, N. Bonod, and E. Popov, "Spectral analysis of three-dimensional photonic jets," Opt. Express **16**(18), 14200–14212 (2008).
26. T. Wang, C. Kuang, X. Hao, and X. Liu, "Subwavelength focusing by a microsphere array," J. Opt. **13**(3), 035702 (2011).
27. R. M. Goldstein, H. A. Zebker, and C. L. Werner, "Satellite radar interferometry: two-dimensional phase unwrapping," Radio Sci. **23**(4), 713–720 (1988).
28. D. C. Ghiglia and M. D. Pritt, *Two-Dimensional Phase Unwrapping: Theory, Algorithms and Software* (Wiley, 1998).
29. J. Arlt and M. J. Padgett, "Generation of a beam with a dark focus surrounded by regions of higher intensity: the optical bottle beam," Opt. Lett. **25**(4), 191–193 (2000).
30. G. M. Philip and N. K. Viswanathan, "Generation of tunable chain of three-dimensional optical bottle beams via focused multi-ring hollow Gaussian beam," J. Opt. Soc. Am. A **27**(11), 2394–2401 (2010).
31. K. T. Gahagan and G. A. Swartzlander, Jr., "Optical vortex trapping of particles," Opt. Lett. **21**(11), 827–829 (1996).
32. T. F. Scott, B. A. Kowalski, A. C. Sullivan, C. N. Bowman, and R. R. McLeod, "Two-color single-photon photoinitiation and photoinhibition for subdiffraction photolithography," Science **324**(5929), 913–917 (2009).
33. T. L. Andrew, H.-Y. Tsai, and R. Menon, "Confining light to deep subwavelength dimensions to enable optical nanopatterning," Science **324**(5929), 917–921 (2009).

1. Introduction

The scattering of light from spherical particles is well described by Mie theory which has been established more than 100 years ago. Mie theory solves Maxwell's equations with a quasi-analytical solution rigorously for that particular geometry [1,2]. In consequence, many of the associated effects expected to emerge have been well studied for long time. Nevertheless, despite this long standing history there is a constant stream of new properties that are revealed and which attract a steady research interest. Most recently, the phenomenon of photonic Nanojets has been disclosed [3]. Photonic Nanojets emerge if micron-sized dielectric spherical objects (cylinders or spheres) are suitably illuminated. A photonic Nanojet manifests as spatially highly confined field localization on the rear side of the sphere (or cylinder) where it lives in the intermediate domain. The localization does not just exist in very close vicinity to the surface in the near-field but stretches beyond. However, since the field is also localized in spatial domains smaller than the usual resolution limit, it is also not suggested to be entirely a far-field phenomenon. Photonic Nanojets emerge as narrow and elongated spots with a high field enhancement. Their existence was first discussed for cylinders in 2004 and for spheres in 2005 [4,5]. Numerous numerical and experimental studies have been reported and two streams of research can be distinguished. On the one hand, the photonic Nanojet itself was subject to investigations and its dependence on key parameters of the system, such as the material parameters of the sphere and background medium, the size of the sphere and the wavelength has been thoroughly investigated [3]. On the other hand, direct applications of photonic Nanojets for sensing and metrology, optical trapping, nano-patterning, and optical data storage have been discussed, which are summarized in an review paper [3]. Photonic Nanojets may also have applicability to the field of biophotonics, such as for probing the internal composition of biological cells [6]. The direct observation of photonic Nanojets is a complicated issue and their observation in the visible has been reported recently [7]. The majority of all these investigations rely however on a linearly polarized plane wave for illumination. There exist only a few studies which apply a focused beam to reduce spot sizes of a photonic Nanojet [8]. In our contribution we close this gap and investigate systematically how a modified and more complex illumination affects the properties of photonic Nanojets.

In our experiments we engineer photonic Nanojets by manipulating the incident wavefront and/or the polarization. We investigate the emerging fields (in amplitude and phase)

#145428 - $15.00 USD Received 5 Apr 2011; revised 29 Apr 2011; accepted 2 May 2011; published 9 May 2011

comprising engineered photonic Nanojets with a high-resolution interference microscope (HRIM). The HRIM allows manipulating the illumination conditions and, at the same time, measuring and monitoring the modified characteristics, such as the wavefront and the polarization of the illumination *in situ*. This is a great advantage since controlling and manipulating the illumination conditions are difficult tasks in other experimental systems, such as a scanning near-field optical or a confocal microscopes, where the illumination is usually restricted to an individual scenario. This advantage of the HRIM comes with the expense that the field is not probed directly behind the sphere but the fields are measured instead in the far-field in an image plane.

We start our investigation by using a linearly polarized plane wave illumination at various wavelengths. This serves as a reference for photonic Nanojets generated by different illumination conditions. We confirm the applicability of our system by comparing experimental results to simulations. The excellent agreement provides confidence that our experimental setup is reliable and allowing measurements with high precision. Since modifying the illumination conditions is more difficult in simulations and since in each case all the illumination details are not accessible, we present further experimental results on the feasibility of the engineering and the beam shaping of photonic Nanojets without simulations.

To this end we systematically modify the illumination condition and investigate its impact on the emerging photonic Nanojets. First, we demonstrate that the phase curvature of the incident wavefront can be used to adjust the axial position of the intensity maximum of the photonic Nanojets, usually called the focal point. Second, we use Bessel beams for illumination and investigate how the specific properties of such beams affect the photonic Nanojets. We distinguish between an on- and an off-axis illumination to discuss the impact of a displacement. Third, we investigate the impact of a particular polarization state on the photonic Nanojets, i.e. we will rely on an azimuthal polarization,. It is shown that this leads to polarization-induced beam shaping that can be applied to generate specific spots.

Overall, we show with this work how to affect specific properties of the photonic Nanojets using suitably shaped illumination which confidently enhances the degree of freedom to consider them in future applications. These implications are discussed throughout the manuscript.

2. Experimental conditions

2.1 High-resolution interference microscopy system setup

High-resolution interference microscopy has been already proven as a powerful tool to characterize micro- and nano-optical elements; such as microlenses and gratings [9,10]. The HRIM operates in transmission by employing a Mach-Zehnder interferometer as shown in Fig. 1. Three single mode polarized laser diodes with different powers and wavelengths are used to investigate the wavelength dependence in the visible spectrum (CrystaLaser, 642 nm: DL640-050-3, 532 nm: IR-GCL-025-S, 405 nm: BCL-040-405-S). A polarizing beam splitter (PBS) divides intensities to be sent in a reference and an object arm with adjustable energy ratio. Half wave plates (HWP) and Glan-Taylor (G-T) polarizers are used to adjust the intensities and to optimize the contrast of the interference fringes. In the reference arm, a piezo-electrically driven mirror is mounted to change the optical path length. The phase distribution of the wave field is obtained by measuring the interference fringes at different mirror positions and employing a classical 5-frame algorithm, which is called Schwider-Hariharan method [11,12]. In this scheme, five frames of the intensity pattern are recorded from which the spatially resolved transmitted phase is reconstructed, each frame being shifted by adding an optical path of $\lambda/4$.

The interferometric function allows measuring and monitoring the wavefronts of the incident illumination beams during the engineering of the photonic Nanojet. In the standard configuration a linearly polarized plane wave illuminates the system under investigation. The object arm can be modified by installing additional components, such as illumination components or polarization controllers into the position of squares one and two of Fig. 1. The

#145428 - $15.00 USD Received 5 Apr 2011; revised 29 Apr 2011; accepted 2 May 2011; published 9 May 2011

sample is mounted on a precision piezo stage with a *z*-scan range of 500 µm and a nominal accuracy of 1 nm (MAD LAB CITY, NANO Z500). This *z*-axis piezo stage is used to precisely define the plane of interest at highest resolution and measure three-dimensional (3D) amplitude and phase field distributions emerging from microstructures by translating the sample together with the illumination.

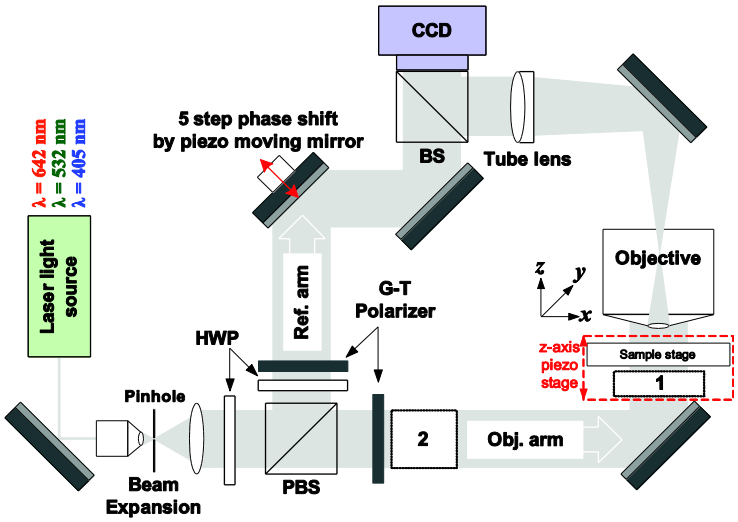

Fig. 1. Schematic of the experimental setup. After divided by the polarizing beam splitter (PBS), a linearly polarized plane wave emerges in both the reference (Ref.) and object (Obj.) arms. In the reference arm, the piezo driven mirror modulates the optical path with five steps of 90° (=λ/4). In the object arm, additional elements to manage polarization and illumination can be used to manipulate the incident illumination. They are placed either in to the position of squares *one* or *two*. Details of the use of such additional components will be discussed in section 2.2.

In general, a high numerical aperture (*NA*) of the observation objective ensures high-resolution of the amplitude and phase measurements. Moreover, high magnification leads to more pixels per area on an image sensor for small fields. While not really useful if intensity only fields are recorded, the phase imaging profits from such oversampling because it is not subjected to the resolution limit [13]. The resolving power for intensity features, i.e. the resolution of an optical imaging system like a microscope, can be limited by factors such as imperfections in the lenses or misalignment. However, there is also a more fundamental limit to the resolution of any optical system which is due to diffraction. An optical system with the ability to produce images with angular resolution as good as the instrument's theoretical limit is said to be diffraction limited [14]. Assuming that optical aberrations in the whole optical setup are negligible, the lateral resolution *d* can be stated as *Abbe limit* (Δx) = $\lambda / 2NA$ [15,16], which has been named in honor of Ernst K. Abbe. Therefore, the nominal lateral resolutions for the 100X / *NA* 0.9 objective (Leica Microsystems, HC PL FLUOTAR), which is equipped in the HRIM, is calculated to be 357 nm at a wavelength of 642 nm. Along the optical axis, the Rayleigh criterion can be applied with the simplified formula derived as $\Delta z = \lambda \cdot n / (NA^2)$, where n is the refractive index of medium [17]. The calculated axial resolution at a wavelength of 642 nm is Δz = 793 nm. At 100X magnification, a pixel on our charge-coupled device (CCD) sensor (Sicon Corporation, CFW1312M camera with SONY ICX205AK image sensor of 1360 x 1024 pixels) corresponds to 46.5 nm in the object plane. This leads to the maximum field of view of the CCD camera of 64 x 48 µm^2, which is sufficiently large to investigate the incident wavefronts and the photonic Nanojets from small microspheres.

#145428 - $15.00 USD Received 5 Apr 2011; revised 29 Apr 2011; accepted 2 May 2011; published 9 May 2011

2.2 Manipulating the field distribution of the illumination

Under standard measurement conditions, an expanded collimated beam which resembles a plane wave with linear polarization along the *x*-axis illuminates the sample as depicted in Fig. 1. By including additional illumination components, such as an aperture, a lens, or a spatial light modulator installed at the position denoted by square #1 in Fig. 1, one can modify the amplitude and/or phase distributions of the incident beam. Two typical examples for such elements as used in our experiments are conceptually shown in Fig. 2, where the sphere is olny shown for completeness at this point in the paper. Figure 2(a) describes the generation of a spherical wavefront by focusing the light with an objective close to the bottom of the sphere. We define a reference plane, called the entrance plane of the sphere, as the plane where the illumination starts to interact with the sphere, hence a plane with its normal parallel to the optical axis and a radius distance away from the spheres center.

A more sophisticated modified illumination is considered, when the central part of a plane-wave illumination is blocked and the amplitude distribution in the focal plane resembles a zeroth-order Bessel function of the first kind in radial direction within finite extentions [14,18]. The finite beam we use for illumination causes a Gaussian apodization in the amplitude distribution and the overall illumination can be analytically represented as a product of a Bessel function and a Gaussian profile. This type of experimental Bessel beams are often called *Bessel-Gauss beams* [19] or focused Bessel beams. Unlike a diffraction-free beam [20,21], such beam carries a finite power and has a finite transverse as well as longitudinal extension due to the fast amplitude decrease of the Gaussian profile. Figure 2(b) illustrates how we generated experimentally a focused Bessel beam (Bessel-Gauss beam) illumination by using a focusing lens with an annular pupil, which creates an annular illumination by blocking the central part of a plane-wave illumination with an opaque disc.

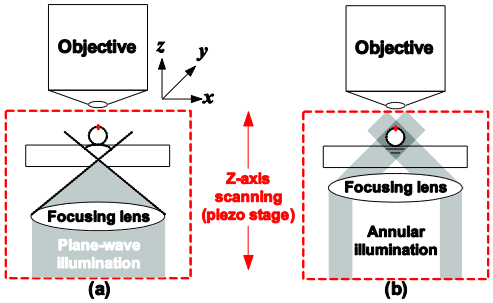

Fig. 2. Use of additional illumination components: (a) a spherical-wavefront illumination is obtained by simply adding a focusing lens at the position denoted by square #1 and either a converging or diverging wavefront can be adjusted by properly placing the foci with respect to the entrance plane of the sphere. (b) A Bessel-Gauss beam as illumination requires to focus an annular incident beam. Elements are fixed on the same piezo stage to be moved together with the sample in order to keep illumination conditions constant during the *z*-axis scanning. The spheres are only shown for completeness at this point in the paper.

When illumination components are inserted underneath the sample into the position of the square labeled with one, they are fixed on the same piezo-stage as the sample. Since a plane-wave incidence on the additional illumination component is guaranteed, the sample together with illumination elements can be scanned in the axial (*z*) direction without changing the illumination conditions. In this manner we assure to measure 3D amplitude and phase distributions with fixed and specific illumination conditions.

Figure 3 shows examples of intensity distributions as measured with the HRIM under various illuminations without a sample, hence only the illumination is shown. Focused Gaussian beams for a low NA (0.15) and a high NA (0.9) are shown in Figs. 3(a) and 3(b), respectively. Figure 3(c) shows the correspondign phase distribution of Fig. 3(b), where the converging and diverging wavefornts can be seen. By blocking 70% of the central part of the entrance pupil, Bessel-Gauss beams are realized and measurements are shown in Figs. 3(d)

#145428 - $15.00 USD Received 5 Apr 2011; revised 29 Apr 2011; accepted 2 May 2011; published 9 May 2011

and 3(e) for low NA (0.15) and high NA (0.9), respectively. Figure 3(f) presents the corresponding phase distribution of Fig. 3(e). As expected, a diamond-like shape in the overlapping region, typical for the interference of two plane waves, is found. Compared to the focused Gaussian beams in Figs. 3(a)–3(c), the longer focal depth of the Bessel-Gauss beams is a clear signature for a strongly suppressed diffraction and the evolution of the phase in space in Fig. 3(f) corresponds to interfering plane waves. Both are properties usually associated with Bessel-Gauss beams. As discussed above, the properties of the Bessel-Gauss beams obtained with our experimental approach are different from Bessel beams obtained for instance by an axicon or a micro-size-opening annular slit [20,21], but are fully sufficient for our study.

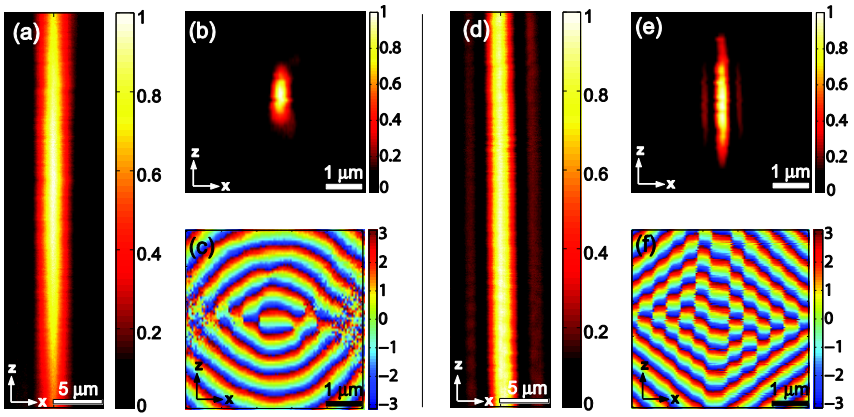

Fig. 3. The *x*-*z* slices of the measured 3D intensity and phase distributions of various illuminations. They are measured without a sample in the HRIM. The intensity distributions of focused Gaussian beams of (a) low NA and (b) high NA and (c) corresponding phase distribution of (b), The intensity distributions of focused Bessel beams of (d) low NA and (e) high NA and (f) corresponding phase distribution of (e). Please note that the scales in low NA and high NA beams are different, which are indicated by a scale bar in each image. Intensities are all normalized.

2.3 Manipulating the polarization of the illumination

Polarization modifying elements, like wave plates or polarization converters, change an incident linear polarization to a specific output polarization. For example, a devoted liquid-crystal (LC) polarization converter can transform linear into radial or azimuthal polarization [22]. In the HRIM a LC radial polarization converter (ARCoptix S.A.) is inserted into the position of square two in Fig. 1 to produce an azimuthal polarization. It assures a doughnut-shape focal spot regardless of the NA of the focusing objective due to nonexistence of longitudinal field component [23]. The focal spot of an azimuthally polarized beam by a low NA (0.15) lens is shown in Fig. 4.

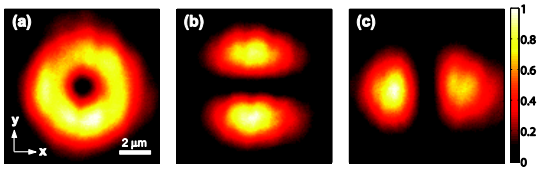

Fig. 4. Measured intensity in the focal plane of a low NA (0.15) lens focusing an azimuthally polarized beam with and without an additional polarizer: (a) without a polarizer a typically doughnut shape intensity appears, (b) with a polarizer parallel to the *x*-axis, and (c) with a polarizer parallel to the *y*-axis symmetric intensity lobs are observed. Image size is 10 x 10 µm^2. Intnsities are all normalized.

#145428 - $15.00 USD Received 5 Apr 2011; revised 29 Apr 2011; accepted 2 May 2011; published 9 May 2011

Figure 4(a) shows the typical doughnut like intensity distribution in the focal plane. When such beams with such polarization state pass through a linear polarizer set just before the focusing lens, decomposition leads to a separation of the spot with an extinction line either parallel or vertical to the axis of the polarizer. Typically, two-half-lobes spots are formed. They are shown in Figs. 4(b) and 4(c) for the polarizer parallel to the *x*-axis and the *y*-axis, respectively.

3. Spectral dependency of photonic Nanojets under plane wave illumination

We start from the standard photonic Nanojet arrangement and a plane-wave illumination for reference. Here, the wavelength is the parameter to be adjusted in the illumination and the spectral dependence of the photonic Nanojet is investigated. Alongside, we verify the results and characteristics of the system by comparing measurement results with simulations. In our experiments we deposit borosilicate glass microspheres of different size (Duke Scientific, n = 1.55 at 642 nm) on a glass substrate (Carl Roth, Borosilicate coverslip with 150-µm thickness) in order to manipulate them properly in the HRIM. The spheres are sufficiently diluted to treat them as isolated. Figure 5 shows the measured intensity distributions of Nanojets in the *x*-*z* and the *x*-*y* planes. The spectral dependence has been explored by applying three different wavelengths available in our instrument. The transverse full width at half maximum (FWHM) spot sizes are measured to be 380 nm, 340 nm, and 230 nm for the wavelength 642 nm, 532 nm, and 405 nm, respectively. We observe that the spot size is directly proportional to the operational wavelength as it could be found in the focal spot of a conventional refractive lens. This is easily understandable as the photonic Nanojet is a non-resonant phenomenon and the light localization in space is simply better the shorter the wavelength is. Taking the ratio of spot size to wavelength provides quantitatively comparable values. In our setup, intensity measurements are subjected to the diffraction limit of the observing objective, whose resolution is give by the Abbe limit; here a HC PL FLUOTAR 100X / NA0.9 objective from Leica Microsystems is used and measured FWHM spot sizes agree with the Abbe limit.

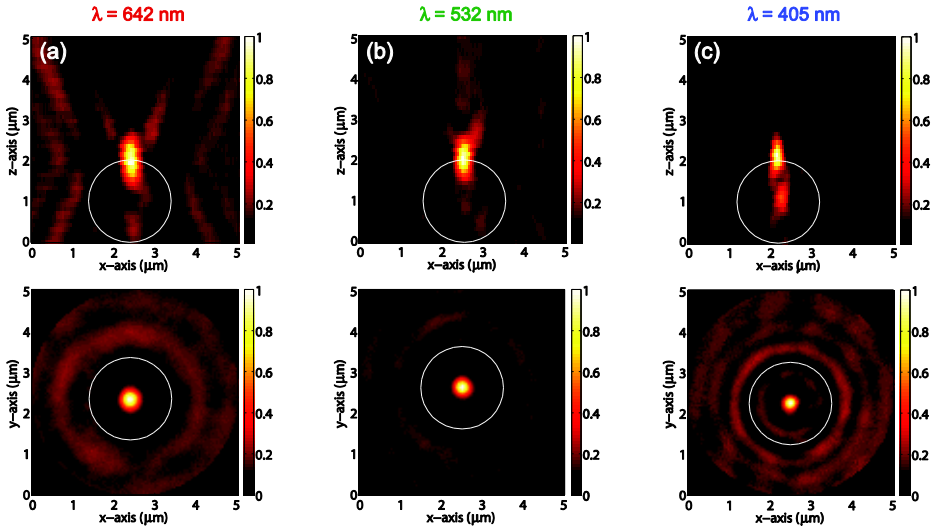

Fig. 5. Measured intensity distributions of photonic Nanojet from a 2-µm glass sphere for different wavelengths: (a) 642 nm, (b) 532 nm and (c) 405 nm. The top surface of the sphere is set to the z = 0 µm. The white circle indicates the 2-µm sphere. Intensities are all normalized.

The simulation of these photonic nanojets has been performed with a computational strategy previously described [24]. In short; Mie theory is used to solve at first the scattering problem of a plane wave at a sphere. The field distribution in a plane 10 µm behind the sphere in the transmission region is calculated at second. Fourier transforming the field, suppressing

#145428 - $15.00 USD Received 5 Apr 2011; revised 29 Apr 2011; accepted 2 May 2011; published 9 May 2011

all spatial frequencies that are not transmitted by the experimental optical system and an inverse Fourier transformation provides the field distribution in this plane as measured in the far field by the HRIM. A free space propagation of the field from that plane to an arbitrarily deviating plane using an angular spectrum approach is used to calculate the field everywhere in space and to compare simulations to experimental results.

Figure 6 shows for all three wavelengths the simulated intensity distributions in the same cross-sections as they have been measured. The transverse FWHM spot sizes are calculated to be 380 nm, 330 nm, and 250 nm for the wavelength 642 nm, 532 nm, and 405 nm, respectively. An excellent agreement is found qualitatively and quantitatively. Most notably, the reduction of the spot size at shorter wavelengths is seen in exactly the same manner as observed in the experiment. This provides confidence that the measured results are not affected by major uncertainties. A further simulation of the more complicated illumination scenario as shown below was not possible since the illumination cannot be characterized with sufficient precision in all parameters as required for a proper simulation. For a plane wave this is much simpler because basically there is no free parameter. Hence in the remainder of the manuscript only experimental results are shown.

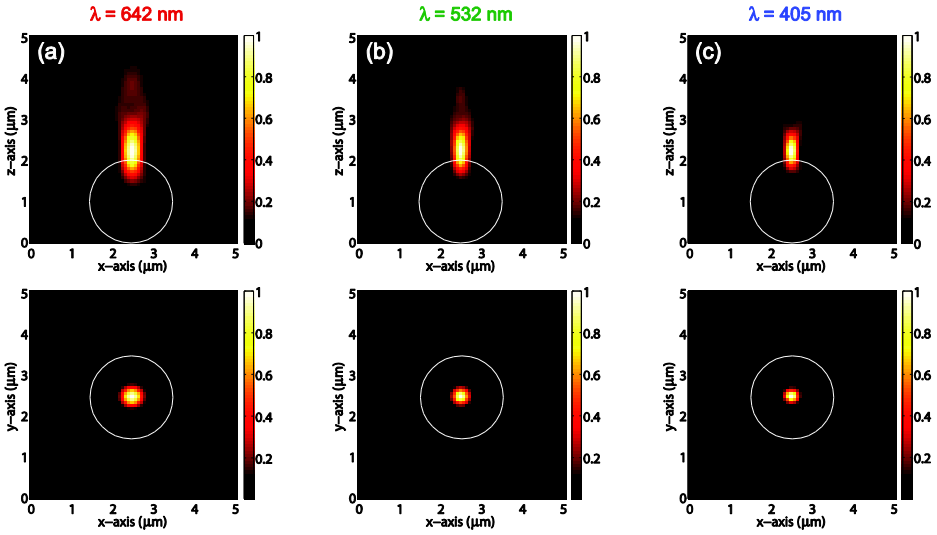

Fig. 6. Corresponding simulations to Fig. 5: (a) 642 nm, (b) 532 nm and (c) 405 nm. They are rigorously calculated by the Mie theory and the scalar propagation technique with the consideration of the NA of the observation system. Intensities are all normalized.

4. Photonic Nanojet by spherical-wave illumnations

As next we apply converging and diverging spherical wavefronts generated by a purposely defocusing to tailor the position of maximal intensity, a quantity which is often linked to the focal length or distance of photonic Nanojets [25,26]. Since there is no evident resonant behavior, for experimental convenience we will work in the following at a single wavelength (642 nm) and a microsphere with larger diameters. All the changes to the field localization while changing the wavelength would have been witnessed in an identical manner when compared to previous investigations. For convenience we recall briefly the situation of focusing for a conventional refractive lens. For a lens we find its focal point moving backward and forward from the principal focal plane found for plane wave illumination depending on the curvature of the incident wavefront. That is possible because the curvature induced by the lens simply adds to the curvature of the illumination. We apply this simple mechanism here to adjust the focal length of the photonic Nanojet.

To generate spherical-wavefront illuminations with different radius of curvatures, we use a 50X / *NA*0.9 objective (Leica Microsystems, HXC PL APO). In HRIM, we can precisely

#145428 - $15.00 USD Received 5 Apr 2011; revised 29 Apr 2011; accepted 2 May 2011; published 9 May 2011

measure and control the radius of curvature (ROC) of waves by holographically recording phase distributions at each defocusing situation. The two dimensional phase distributions at the entrance pupil plane are shown in Figs. 7(a)–7(d), where target ROCs were 50 μm, 15 μm, −15 μm, and −50 μm, respectively. The ROC of a converging spherical wavefront is defined to have a negative value. Figure 7(e) shows wavefront profiles and measured ROCs derived from Figs. 7(a)–7(d), which are obtained by a 2D phase unwrapping process [27,28]. ROCs are found to be 52.7 μm, 14.9 μm, −17 μm, and −48.3 μm, respectively. Diverging spherical wavefronts in Figs. 7(a) and 7(b) show undesired spherical aberrations and ripples in the wavefornt profiles. These aberrations are a result of the coverglass correction of the microscope objective which only correctly applies for the lower half space of the illumination conditions in the experimental geometry. These manipulated wavefronts were used to engineer the photonic Nanojets.

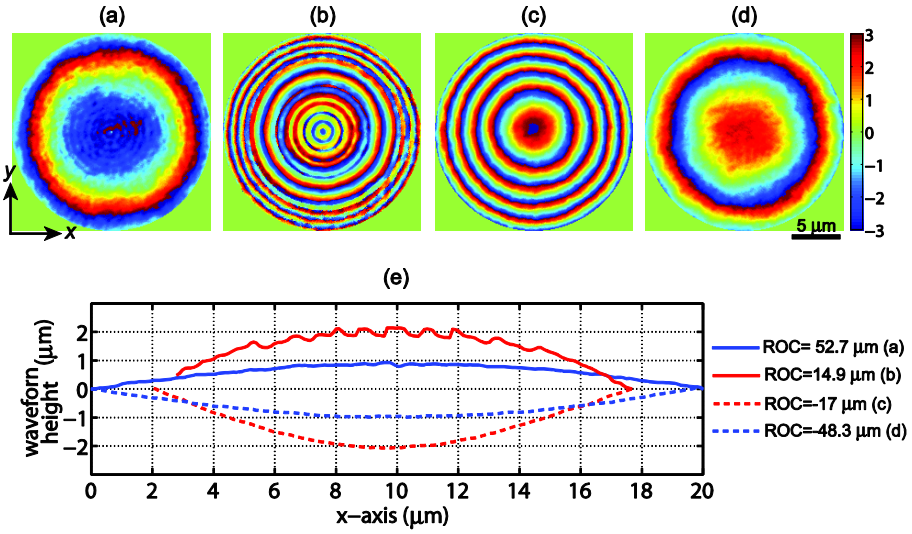

Fig. 7. Measured 2D phase distributions of spherical waveforns at the entrance pupil plane of the sphere, which are used to engineer photonic Nanojets: (a) ROC = 52.7 μm, (b) ROC = 14.9 μm, (c) ROC = −17 μm, and (d) ROC = −48.3 μm. The colorbar scale is radian. (e) Profiles through the center of the wavefront from (a) to (d).

Figure 8 shows the longitudinal intensity distributions of photonic Nanojets generated by a glass sphere with a diameter of 12 μm. Engineered Nanojets are compared to the Nanojet formed by a plane-wave illumination as shown in Fig. 8(a).

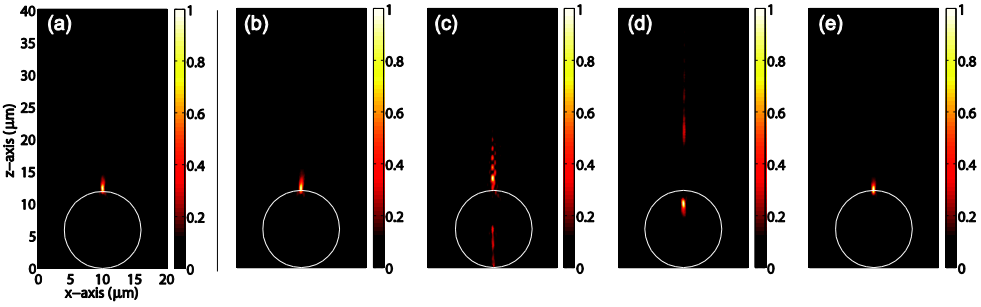

Fig. 8. Longitudinal intensity maps of photonic Nanojets generated by a 12-μm glass sphere. (a) Reference measurement with a plane-wave illumination. Engineered Nanojets when the sphere is illuminated by (b) diverging wavefront with a ROC of 52.7 μm, (c) diverging wavefront with a ROC of 14.9 μm, (d) converging wavefront with a ROC of −17 μm, and (e) converging wavefront with a ROC of −48.3 μm. The white circle indicates the 12-μm sphere. Intensities are all normalized and the scale of all images is the same.

#145428 - $15.00 USD Received 5 Apr 2011; revised 29 Apr 2011; accepted 2 May 2011; published 9 May 2011

As one would expect from a classical lens system, spherical wavefronts of different curvatures shift the focal plane of the Nanojet. For instance, diverging spherical wavefronts pushes the Nanojet spot away from its principal focal plane (the shadow-side surface of the sphere) towards the far field as shown in Fig. 8(c). This phenomenon was observed with various spheres of different sizes. The corresponding spot sizes were generally found bigger than that of a standard Nanojet created by a plane-wave illumination. Within a certain range, this mechanism allows to adjust the working distance of Nanojets. It has to be furthermore stressed that this displacement of the photonic Nanojets is stronger the smaller the absolute value of the ROC is. The larger this value is, the stronger the illumination resembles a plane wave for which the photonic Nanojet is bound to the surface. Continuously adjusting the ROC of the illumination allows for tuning of this distance, as shown in the measurement, in certain intervals. This may have tremendous implications for the use of such photonic Nanojets for high resolution microscopy or also for optical tweezers. There, a free manipulation of the focal position by a suitably chosen illumination would enable the manipulation of trapped objects in space.

5. Photonic Nanojet generated by Bessel-Gauss beams

A Bessel beam is a non-diffracting beam [20,21] with a planar phase evolution in space and a radial amplitude distribution corresponding to a Bessel function. Mathematically, these beams are slightly pathologic since they are infinite extended in space, each ring of the Bessel beam carries the same amount of energy which adds up to infinity, the phase among adjacent rings differs exactly by π, and the Fourier spectrum of such Bessel beam is an infinitely thin ring. Therefore, perfect Bessel beams are inaccessible in a true experiment and their spatial distribution can only be sufficiently approximated within some finite distance. These approximations are experimentally acquired by focusing the parallel annular illumination as explained in the section 2.2. As can be seen in Fig. 9, where the intensity and the phase in selected cross-sections of the illumination used in the experiment are shown, the ideal Bessel beam is fully sufficient approximated and the beam stretches non-diffracting a much larger spatial domain than that which is of experimental relevance.

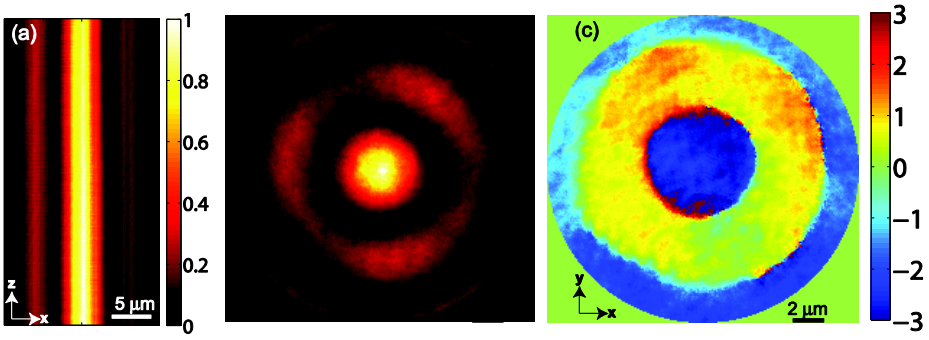

Fig. 9. (a) Measured *x*-*z* intensity distribution of a low *NA* (0.15) focused Bessel beam (the image size is 40 x 20 μm^2). At the plane of z = 0 μm, (b) the *x*-*y* intensity and (c) the *x*-*y* phase distributions are recorded (the image size is 20 x 20 μm^2). Intensities are all normalized. The FWHM size of the central lobe is measured to be 4 μm.

As shown already in Fig. 3(f), the wavefronts of such beams are planar but the transverse extension is not continous. Figure 9(c) shows a transverse phase distribution, where one observes the discrete wavefronts and their phase difference of π in adjacent rings. Here, our interest is to exploit such discrete-wavefront illuminations. Although there are various experimental configurations, we generalized them and distinguish three cases: (1) a sphere smaller than the central lobe of the Bessel-Gauss beam placed on-axis, (2) a sphere larger than the central lobe placed on-axis, and (3) a sphere placed within two lobes of such a beam (off-axis).

#145428 - $15.00 USD Received 5 Apr 2011; revised 29 Apr 2011; accepted 2 May 2011; published 9 May 2011

The size of the central lobe of the focused Bessel beam depends on the NA of the focusing lens when the size of the annular pupil is fixed. In our case the central obstraction is 70% of the entrance pupil. Generally, the focal spot that is observed with such illumination is slightly smaller than the focal spot found for the focused Gaussian beams at the same NA since the Bessel function leads to the narrower central lobe than Airy function [14,18]. In order to illuminate the entire surface of the sphere with the central lobe of a Bessel-Gauss beam, we work with a low NA generated by an objective with *NA* = 0.15. The resulting beam characteristics are shown in Fig. 9. The FWHM size of the central lobe is measured to be 4 μm.

5.1 On-axis Bessel-Gauss beam

In the first experiment the width of the central lobe is larger than the scattering object, a sphere with a diameter of 2 μm. The longitudinal intensity distribution of the generated Nanojet for this case is shown in Fig. 10(a) in a logarithmic scale. Since scattered fields out of the sphere are weak and not observable with a linear intensity scale, a logarithmic scale is used to emphasize the details in low intensity regions. Figure 10(b) is a close-up image in the vicinity of the sphere with a linear scale of intensity. The spot size is found to be 360 nm, which stays similar to a plane-wave case (380 nm), and the intensity maximum position is found on the rear side surface of the sphere. Since the continuous plane wavefront illuminates the entire surface of the 2-μm sphere, this leads to comparable results as for the plane-wave illumination, as could have been anticipated. Moreover, the self-healing property of the Bessel beam is demonstrated by its rebirth after around 10 μm in the *z*-axis, clearly identified in Fig. 10(a).

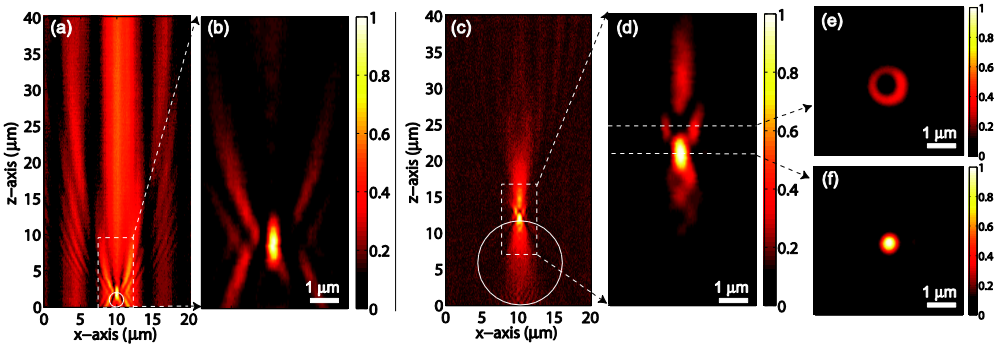

Fig. 10. (a) Measured *x*-*z* intensity distribution of a Nanojet produced by a 2-μm sphere when the central lobe of the Bessel beam is larger than the sphere and (b) the close-up image of (a). (c) Measured *x*-*z* intensity distribution of a Nanojet produced by a 12-μm sphere when the central lobe of the Bessel beam is smaller than a sphere and (d) the close-up image of (c). (e) The *x*-*y* intensity image at z = 13 μm (a dark focus) and (f) the *x*-*y* intensity image at z = 12 μm (a bright focus). The intensity levels in (a) and (c) are displayed with a logarithmic scale in order to visualize the scattered fields out of the sphere and especially self-healing of the Bessel beam in (a). The white circle indicates the 2-μm sphere in (a) and the 12-μm sphere in (c), respectively. Intensities are all nomalized.

Now, we examine the Nanojet when the central lobe is smaller than the spheres' diameter which is chosen to be 12 μm now. The measurements are shown in Figs. 10(c)–10(f). The dominating spot of the photonic Nanojet is formed, as usual, on the surface of sphere with strong intensity confinement. Close to this unique intensity distribution of a Nanojet the emergence of a hollow ring is observed. A weakly ring-shaped intensity lobe, i.e. a dark focus surrounded by regions of higher intensity, is found between two bright spots. The physical origin of such phenomenon is presumed to be the same mechanism as of an *optical bottle beam* [29,30]. The π phase difference between the central lobe and the 1st lobe of the Bessel beam serves as the annular-shape illumination mask for either phase or amplitude. Similar consequences have been found in Fig. 8(c) which can be seen as a chain of optical bottle

#145428 - $15.00 USD Received 5 Apr 2011; revised 29 Apr 2011; accepted 2 May 2011; published 9 May 2011

beams due to the spherical-aberration-induced annular illumination beams. The formation of such region with a low intensity surrounded by bright regions could be exploited in many interesting applications. Examples would be the trapping of particles with a lower index than its surrounding which are known to be pushed towards regions of low intensity [31] or for combining possibly microscopes using photonic nanojets with the advantages of a stimulated emission deplection (STED) microscope.

5.2 Off-axis Bessel-Gauss beam

For the case of an off-axis Bessel-beam illumination that breaks the axial symmetry of the arrangement, a microsphere is placed in between two annulus of an incident Bessel beam, which have a phase difference of π. Since a 2-μm sphere is too small to significantly probe the fields from the two lobes of the given Bessel beam, we work with a 4-μm sphere under the same experimental conditions as pointed out for Fig. 10. The optical axis of illumination is shifted away from the sphere (off-axis geometry) as shown in Fig. 11(a). The dark ring associated with the phase difference divides the illuminating wavefronts in two and finally leads to the emergence of a two-spot Nanojet as impressively shown in Fig. 11. The longitudinal slices of the measured 3D intensity data are given in Figs. 11(c)–11(e). Separation of two bright spots is 220 nm at FWHM, which is about 40% smaller than the measured Nanojet spot size at the wavelength of 642 nm. These phenomena are observed with spheres of different sizes and focused Bessel beams of different numerical apertures. Here we experimentally demonstrated the feasibility of beam shaping by specific illuminations when intensity distributions and wavefronts are discontinuous. As we can see in Figs. 11(a), 11(b) and 11(e), the remaining parts of the illuminating beam outside the sphere are still relatively strong. Nevertheless, the phenomenon would be well suited for specific applications such as trapping or patterning. Since the Bessel beam has a self-healing characteristic, manipulating light from the unwanted lobes of the Bessel beam becomes difficult. For many applications only the ratio of confined light intensity to background intensity is important which remains still high in our case. This qualifies our approach to be used for trapping for instance.

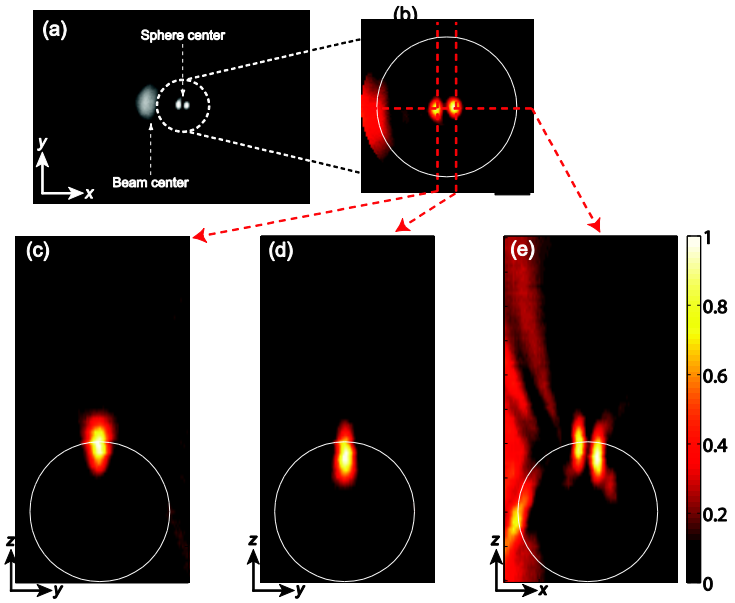

Fig. 11. Measured intensity distributions of the two-spot Nanojet from the 4-μm sphere by off-axis Bessel-Gauss beam illumination: (a) a grayscale CCD image of the off-axis Bessel beam and two-spot Nanojet, (b) the *x*-*y* slice of the 3D intensity distributions at the top of the sphere (c) the *y*-*z* slice at the center of the left spot, (d) the *y*-*z* slice at the center of the right spot and (e) the *x*-*z* slice of the two spots. The white circle indicates the 4-μm sphere. Intensities are all normalized.

#145428 - $15.00 USD Received 5 Apr 2011; revised 29 Apr 2011; accepted 2 May 2011; published 9 May 2011

6. Beam shaping of Nanojet by polarization engineering

As demonstrated in section 2 [see Fig. 4], a cylindrical vector beam with an azimuthal polarization is well know to form a doughnut-shape spot and a two-half-circle spot when it is focused. These particular spots do not have side lobes and we can readily control the finite extension of the spot at the entrance plane of the sphere by varying the NA of the focusing lens. Results of experiments with different relations of illumination spot size and sphere size are given in Fig. 12. The grayscale CCD images of various illumination spots and engineered Nanojet spots for different polarization conditions and sphere sizes are shown. Figure 12(a) shows illumination spots recorded at the entrance plane of the sphere without a sphere, which is identical to Fig. 4.

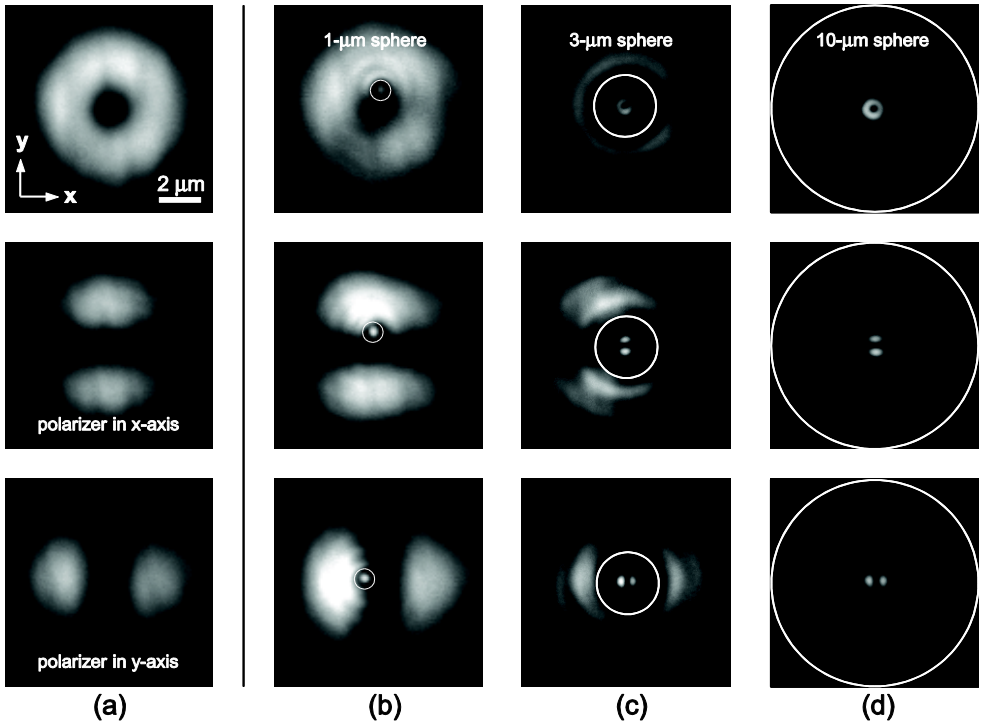

Fig. 12. Grayscale CCD images of particular illumination spots and corresponding engineered Nanojet spots by spheres of different size: (a) illumination spots at the entrance plane without a sphere (same as Fig. 4), (b) with the 1-μm sphere, (c) with the 3-μm sphere, and (d) with the 10-μm sphere. The white circle indicates microspheres. Image size is 10 x 10 μm^2.

When the sphere is small, for instance, a 1-μm sphere as in Fig. 12(b), only a single section of the illumination, either a bright or a dark part, dominates. A standard Nanojet with one spot is observed when setting the sphere in the bright intensity area where the sphere experiences locally a plane wave illumination. In the case that such a small object is located in the dark part of the illumination, Nanojets are not formed and the object is not visible because the sphere is not illuminated with a noticeable strength. Figure 12(c) shows the case of a 3-μm sphere, which is covered by both dark and bright parts of the illumination. A hollow Nanojet and a two-spot Nanojet are generated by corresponding illuminations when polarizations depicted in Fig. 4 are used. Since the size of the sphere is smaller than the illumination spot, a part of the direct illumination is still detectable in the focal plane of the Nanojet as shown in Fig. 12(c). When the sphere is much larger in size than the full extension of the illumination spot, the photonic Nanojet takes the form of the illumination as presented in Fig. 12(d). To profit best from the beam shape control by polarization the size of the sphere should be larger than or eaqual to the illumination spot size.

#145428 - $15.00 USD Received 5 Apr 2011; revised 29 Apr 2011; accepted 2 May 2011; published 9 May 2011

Figure 13 presents the transverse and longitudinal intensity distributions of the hollow Nanojet created by the 10-µm sphere, which is shown in the top of Fig. 12(d). They demonstrate the extinction of bright spots at the center along the optical axis. The FWHM size of this extinction gap of the hallow Nanojet and the two-half-circles Nanojet is measured to be around 200 nm, which is 50% smaller than the size of a standard Nanojet spot for a given sphere size and wavelength. A possible application for such two-spot Nanojets would be direct-write lithography. Scanning these particular intensity distributions of Nanojets can allow creating structures with line widths that are much smaller than the diffraction limit but at larger distance. Moreover, super-resolution lithography applicationes can be imagined when two wavelengths are used illumination, such as done in STED microscopy and absorbance modulation assisted lithography [32,33].

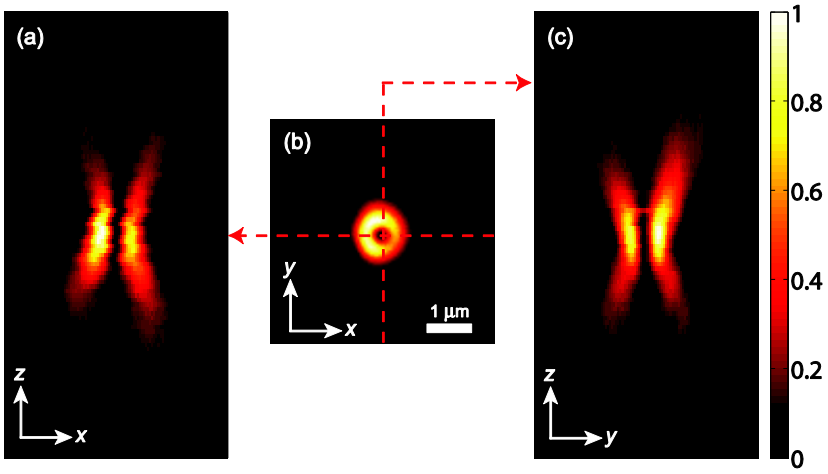

Fig. 13. 3D intensity measurements of the hollow Nanojet generated by the 10-µm sphere same as the top image of Fig. 12(d): (a) the *x*-*z* slice, (b) the *x*-*y* slice at the focal plane, and (c) the *y*-*z* slice of 3D measurement data. The FWHM size of the central dark area is measured to be around 200 nm. The illumination here was an azimuthally polarized beam.

8. Conclusions

In conclusion, we have investigated in this work on experimental grounds how different illumination conditions affect the properties of photonic Nanojets that emerge on the rear side of dielectric microspheres. We have employed in this work a high-resolution interference microscope to access the amplitude and phase of the photonic Nanojets. It was largely found that the properties of photonic Nanojets are dominated by physical optics effects. In consequence, many phenomena can be understood by applying conventional refractive optical arguments for their understanding.

In our investigations we studied at first the spectral dependency of photonic Nanojets for a plane wave illumination; both experimentally and numerically. To this end we presented results for three different wavelengths; namely red at 642 nm, green at 532 nm and blue at 405 nm. Simulations show excellent agreement with experiments which guarantees that the performance of our experimental system is reliable. The spectral dependency of different parameters describing the photonic Nanojets indicated a clear scaling effect that is found in the imaging formation when no resonant effects are expected to be involved.

When the Nanojet has its intensity maximum directly on the back surface of the sphere, it is rather complicated to use it in applications since the spatial proximity of the sample and the sphere constitutes an obstacle. We have therefore shown that the spot position can be engineered by applying spherical wavefront for the illumination with different radius of curvature. We found that a diverging spherical wavefronts can push the focal plane several micrometers away from the surface of the sphere at the expense of a slightly larger spot size.

#145428 - $15.00 USD Received 5 Apr 2011; revised 29 Apr 2011; accepted 2 May 2011; published 9 May 2011

The interesting case of using a non-diffractive beam for illumination was studied by relying on a Bessel-Gauss beam. We considered two scenarios: when the central lobe of the Bessel beam is larger or smaller than the sphere. The former leads to a similar response as found for a plane-wave illumination. In the latter case, a photonic Nanojet spot is generated that is larger than the central lobe of the illuminating Bessel-Gauss beam and which resembles an optical bottle beam.

We demonstrated furthermore that an off-axis Bessel-Gauss beam illumination can create a two-spot photonic Nanojet, if the sphere is placed in between two intensity lobes of the Bessel beam. We applied polarization-induced beam shaping to create specific illumination spots, such as a doughnut shape and a two-half-circle shape. The field distribution of the photonic Nanojets surprisingly resembled the illumination in its entire shape and transformed itself to a hollow photonic Nanojet and a two-spot Nanojet for the aforementioned cases. For the case where two adjacent photonic Nanojets were created, the separation between the two spots was approximately 200 nm at a wavelength of 642 nm, which is smaller than the diffraction limited spot size of the highest NA objective. Our study clarifies different technical aspects of photonics Nanojet which are important for its use in different structuring techniques or ultra-resolution applications.

Acknowledgment

The research leading to these results has received funding from the European Community's Seventh Framework Programme FP7-ICT-2007-2 under grant agreement n° 224226.

#145428 - $15.00 USD Received 5 Apr 2011; revised 29 Apr 2011; accepted 2 May 2011; published 9 May 2011